Heat Mass Transfer (2013) 49:973–984
DOI 10.1007/s00231-013-1143-x

ORIGINAL

A porous media theory for characterization of membrane blood oxygenation devices

Yoshihiko Sano · Jun Adachi · Akira Nakayama

Received: 12 March 2012 / Accepted: 13 March 2013 / Published online: 23 March 2013

Abstract A porous media theory has been proposed to characterize oxygen transport processes associated with membrane blood oxygenation devices. For the first time, a rigorous mathematical procedure based a volume averaging procedure has been presented to derive a complete set of the governing equations for the blood flow field and oxygen concentration field. As a first step towards a complete three-dimensional numerical analysis, one-dimensional steady case is considered to model typical membrane blood oxygenator scenarios, and to validate the derived equations. The relative magnitudes of oxygen transport terms are made clear, introducing a dimensionless parameter which measures the distance the oxygen gas travels to dissolve in the blood as compared with the blood dispersion length. This dimensionless number is found so large that the oxygen diffusion term can be neglected in most cases. A simple linear relationship between the blood flow rate and total oxygen transfer rate is found for oxygenators with sufficiently large membrane surface areas. Comparison of the one-dimensional analytic results and available experimental data reveals the soundness of the present analysis.

List of symbols

A	Cross-sectional area of the blood flow passage
$Aint$	Interface between the fluid and membrane phases
$a_{b,ox}$	Specific surface area
c	Dissolved oxygen concentration
c^*	$c^* = \langle c \rangle^b / c_{ref}$: Dimensionless dissolved oxygen concentration
c_{ref}	$c_{ref} = \alpha p_{ref}$: Reference oxygen concentration at $S = 0.5$
$[c]_H$	Hemoglobin concentration
$d_{b,ox}$	Outer and inner diameters of the hollow fiber
$D_{b,ox,m}$	Oxygen diffusion coefficient
$D_{b\ dis}$	Oxygen dispersion coefficient
$h_{b,ox}$	Mass transfer coefficient
$h_{t\ b,ox}$	Effective mass transfer coefficient
h_{bv}	$h_{bv} = a_b h_b$: Volumetric mass transfer coefficient
K	Permeability
L	Effective length of the oxygenator chamber
n	Exponent associated with Hill's equation
n_i	Unit vector pointing outward from the fluid side to membrane side
Na	$Na \equiv u_b^2 / \varepsilon_b D_{b\,dis} h_{bv}$: Dimensionless number
p	Pressure
p_{ox}	Oxygen partial pressure
$p_{ox\,in}$	Oxygen partial pressure at blood phase inlet
$p_{ox\ \sup}$	Oxygen partial pressure at oxygen phase inlet
p_{ref}	Reference oxygen partial pressure at $S = 0.5$
Q_b	$Q_b = A u_b$: blood flow rate
Q_{ox}	Total oxygen transfer rate
$Q_{ox\,th}$	Total oxygen transfer rate with infinite flow path length
$S(c)$	Oxygen saturation
Sc	$Sc = \nu / D$: Schmidt number
Sh	Sherwood number
t	Time
t_m	Membrane thickness
u_b	Dacian velocity of the blood
u_{ox}	Dacian velocity of the oxygen

Y. Sano · J. Adachi · A. Nakayama (✉)
Department of Mechanical Engineering, Shizuoka University, 3-5-1 Johoku, Hamamatsu 432-8561, Japan
e-mail: tmanaka@ipc.shizuoka.ac.jp

A. Nakayama
School of Civil Engineering and Architecture, Wuhan Polytechnic University, Wuhan 430023, Hubei, China

u_i Velocity vector
V Representative elementary volume
x Axial coordinate
x^* $x^* = h_{bv}x/u_b$: Dimensionless coordinate

Greek symbols

α Oxygen solubility
ε Volume fraction
μ Viscosity
ν Kinematic viscosity
ρ Density
η_{th} $\eta_{th} \equiv \frac{Q_{ox}}{Q_{ox\,th}}$: Oxygenator efficiency

Special symbols

$\tilde{\phi}$ Deviation from intrinsic average
$\langle\phi\rangle$ Darcian average
$\langle\phi\rangle^{b,ox,m}$ Intrinsic average

Subscripts and superscripts

b Blood
ox Oxygen
m Membrane
dis Dispersion
f Fluid
sup Supply
in Inlet

1 Introduction

Hollow fiber membranes are widely used in most blood oxygenators, in which thousands of small polymer tubes are arranged to allow oxygen gas to flow through the inside (lumen side) of the hollow fibers, and blood to flow outside (shell side) of them. Various types of membrane blood oxygenation devices are available today. Some are used to provide temporal cardiopulmonary bypass during open-heart surgery, while others are used for extracorporeal membrane oxygenation to support cardiopulmonary function for the patients with respiratory failure. In such oxygenators, the blood paths may be locally parallel or may have some angle to the oxygen flow within the hollow fibers. In some compact oxygenators, the blood flow paths are mostly radial across the bundles of hollow fibers. There, the blood first enters axially through the core of the oxygenator chamber and then is redirected to pass radially crossing over the bundle of the hollow fibers.

Naturally, the local blood flow field within the oxygen chamber controls the oxygen transfer rate between the oxygen gas in the lumen side of the hollow fibers and the blood plasma flowing though the interstitial spaces in the shell side of the hollow fibers. Thus, it is essential to reveal a local blood flow field in the membrane oxygenator device, so as to characterize the device for its possible improvement in the oxygen transport. Guzman et al. [1] treated an intravenous membrane oxygenator device numerically, assuming angular symmetry and dividing the device in periodic angular sections. A method similar to this was adopted by Guzman et al. [2] to predict flow and oxygen transport characteristics and performance of an intravenous membrane oxygenator device. In most practical cases, such symmetry conditions are not realized. The presence of thousands of hollow fibers makes it practically impossible to apply direct CFD approaches to such complex membrane oxygenator devices.

Hewitt et al. [3, 4] proposed a mathematical model based on a lumped compartment approach. They used empirical correlations for mass transfer coefficient and proved that the model can capture various characteristics of gas exchange processes. A similar approach was taken by Federspiel et al. [5, 6] to find that the results based on the lump method are quite sensitive to a particular choice of the empirical correlation. In reality, the mass transfer coefficient locally depends on the velocity field, so that both velocity and concentration distributions must be sought together to characterize the oxygen transport processes.

Under the situations, in which thousands of hollow fibers are present in an oxygenator chamber, the concept of local volume-averaging theory, namely, VAT, widely used in the study of porous media [7–11] may be useful, as successfully exploited by Sano and Nakayama [12] to analyze mass diffusion and ultrafiltration processes associated with dialysis. In VAT, one uses a grid system, which is just fine enough to resolve macroscopic blood flow and concentration fields. Thus, hollow fiber elements are not resolved but are modeled as a porous medium. This theory of porous media appears to be most appropriate for treating transport phenomena within hollow fibers since it contains fewer assumptions as compared to existing models. In most compact oxygenators in practice, the blood flow directions are not parallel to the hollow fibers. Naturally, both blood flow field and oxygen concentration field exhibit quite complex three-dimensional patterns, due to the presence of the hollow fibers. Therefore, a three-dimensional version of the volume averaged governing equations based on a porous media approach is required to reveal local flow and concentration fields.

Catapano et al. [13] carried out an experiment to investigate mass and momentum transport in blood oxygenators using membrane oxygenation modules with water, and correlated the results using porous media parameters. A CFD study was conducted by Zhang et al. [14] to characterize membrane blood oxygenation devices, modeling the bundle of the hollow fibers as a porous medium. They are successful in deriving the oxygen conservation

equation considering its balance within an elementary control volume. However, in their study, various assumptions were introduced including one for the oxygen effective diffusion coefficient. Possible effects of mechanical dispersion and tortuosity of diffusivity on the oxygen transport have not been considered in their model.

In this paper, a rigorous mathematical development based on the volume-averaging theory is presented so as to establish a complete set of the volume-averaged governing equations for fiber membrane blood oxygenation devices. The relative magnitudes of oxygen transport terms, namely, convection, diffusion and interstitial transport terms will be made clear, introducing a dimensionless parameter which measures the distance the oxygen gas travels to dissolve in the blood as compared with the blood dispersion length. As a first step towards a complete three-dimensional numerical analysis, one-dimensional steady case is investigated analytically to model typical membrane blood oxygenator scenarios.

2 Volume averaging theory, volume fractions and specific areas of oxygenator

Figure 1 schematically shows a membrane blood oxygenation device, in which only outer hollow fibers are shown for clarity. The blood oxygenator utilizes thousands of hollow fibers of polymer membrane. The oxygen flows through the inside lumen of these hollow fibers, whereas the blood flows outside (shell-side) through the interstitial spaces in the packed fiber chamber. In the figure, a parallel flow oxygenator is illustrated for simplicity, in which the blood and oxygen flow in the same direction in parallel. However, in most oxygenators, blood flow patterns are quite complex, crossing over the bundle of hollow fibers. The blood flow paths may be radial or fully three-dimensional. Thus, it is essential to establish a reliable numerical tool so as to reveal such complex blood flow field and oxygen concentration field. Only with such a numerical tool, one may be able to optimize membrane blood oxygenation devices.

Direct numerical simulations of three dimensional flow and concentration fields within packed fiber chambers are practically infeasible, because of the presence of thousands of hollow fibers. Hence, a porous media approach is used in this study to derive a complete set of the volume-averaged governing equations for membrane blood oxygenation devices. The following procedure introduced by Nakayama and Kuwahara [11] for a general bioheat transfer model may readily be extended for the case of membrane blood oxygenation system.

One considers a local control volume V in a fluid-saturated porous medium, as shown in Fig. 2, whose length scale $V^{1/3}$ is much smaller than the macroscopic characteristic length $V_c^{1/3}$, but, at the same time, much greater than the microscopic characteristic length (see e.g. Cheng, [7]; Nakayama [9]). Under this condition, the volume average of a certain variable ϕ is defined as

$$\langle \phi \rangle = \frac{1}{V} \int_{V_f} \phi dV \tag{1}$$

Another average, namely, intrinsic average, is given by

$$\langle \phi \rangle^f = \frac{1}{V_f} \int_{V_f} dV \tag{2}$$

where V_f is the volume space which the fluid phase (blood or oxygen) occupies. Obviously, two averages are related as $\langle \phi \rangle = \varepsilon_f \langle \phi \rangle^f$, where $\varepsilon_f = V_f/V$ is the local volume fraction of the phase in consideration.

A variable is decomposed into its intrinsic average and the spatial deviation from it:

$$\phi = \langle \phi \rangle^f + \tilde{\phi} \tag{3}$$

All dependent variables in the microscopic governing equations for the blood, oxygen and membrane phases will be decomposed in this manner. Thus, one utilizes the following spatial average relationships:

$$\langle \phi_1 \phi_2 \rangle^f = \langle \phi_1 \rangle^f \langle \phi_2 \rangle^f + \left\langle \tilde{\phi}_1 \tilde{\phi}_2 \right\rangle^f \tag{4}$$

$$\left\langle \frac{\partial \phi}{\partial x_i} \right\rangle = \frac{\partial \langle \phi \rangle}{\partial x_i} + \frac{1}{V} \int_{A_{\text{int}}} \phi n_i dA \quad \text{or}$$
$$\left\langle \frac{\partial \phi}{\partial x_i} \right\rangle^f = \frac{1}{\varepsilon_f} \frac{\partial \varepsilon_f \langle \phi \rangle^f}{\partial x_i} + \frac{1}{V_f} \int_{A_{\text{int}}} \phi n_i dA \tag{5a, b}$$

and

$$\left\langle \frac{\partial \phi}{\partial t} \right\rangle = \frac{\partial \langle \phi \rangle}{\partial t} \tag{6}$$

A_{int} represents the interfaces between the fluid and membrane matrix within the local control volume. Note n_i is the unit vector pointing outward from the fluid side to membrane matrix side.

In applying the foregoing porous media approach to an oxygenator, one defines individual velocities and species concentrations to the three phases, namely, the blood, oxygen gas and membrane phases. Each phase is treated as a continuum filling the entire space of the oxygenator chamber. Thus, three phases share the same space but with different volume fractions. Assigning the subscripts, b, ox and m to the blood phase, oxygen gas phase and membrane phase, respectively, the following relations can be found for the volume fractions ε_b, ε_m, ε_{ox}, the specific area of the

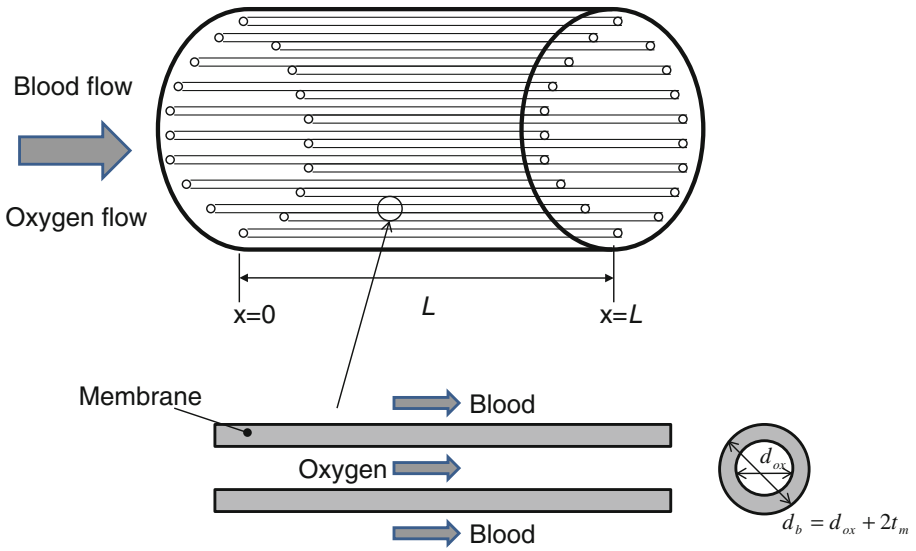

Fig. 1 Oxygenation system

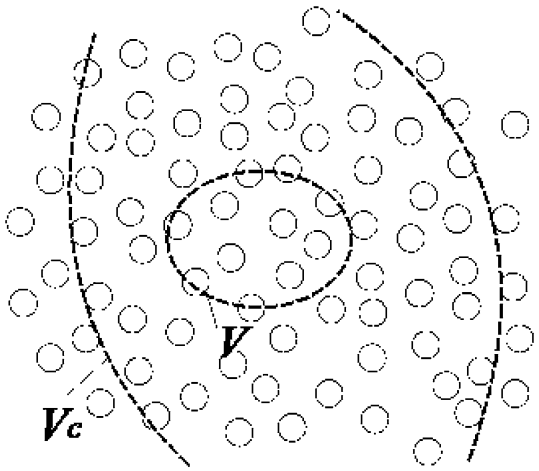

Fig. 2 Control volume in a porous medium

blood compartment a_b and that of the oxygen compartment a_{ox}:

$$\varepsilon_b = 1 - \frac{N\frac{\pi}{4}d_b^2}{A} \tag{7a}$$

$$\varepsilon_m = \frac{\frac{\pi}{4}\left(d_b^2 - (d_b - 2t_m)^2\right)}{\frac{\pi}{4}d_b^2}(1-\varepsilon_b) = 4\frac{t_m}{d_b}\left(1 - \frac{t_m}{d_b}\right)(1-\varepsilon_b) \tag{7b}$$

$$\varepsilon_{ox} = (1-\varepsilon_b)\left(1 - 4\frac{t_m}{d_b}\left(1 - \frac{t_m}{d_b}\right)\right) \tag{7c}$$

$$a_b = \frac{4(1-\varepsilon_b)}{d_b} \tag{8a}$$

$$a_{ox} = \frac{4(1-\varepsilon_b)}{d_b}\left(1 - 2\frac{t_m}{d_b}\right) \tag{8b}$$

Note that N is the number of hollow fibers while A is the cross-sectional area of the oxygenator chamber. The membrane thickness, the inner and outer diameters of the hollow fiber are indicated by t_m, d_b and $d_{ox} = d_b - 2t_m$, respectively.

3 Macroscopic governing equations

The microscopic governing equations, namely, the continuity, momentum and dissolved oxygen conservation equation in the blood phase can be written as follows:

$$\frac{\partial u_j}{\partial x_j} = 0 \tag{9}$$

$$\rho_b \frac{\partial u_i}{\partial t} + \rho_b \frac{\partial u_j u_i}{\partial x_j} = -\frac{\partial p}{\partial x_i} + \mu_b \frac{\partial^2 u_i}{\partial x_j^2} \tag{10}$$

$$\frac{\partial c}{\partial t} + \frac{\partial u_j c}{\partial x_j} = \frac{\partial}{\partial x_j} D_b \frac{\partial c}{\partial x_j} + So \tag{11}$$

where D_b [m^2/s] is the diffusivity of the dissolved oxygen in the blood. c [m^3ox/m^3blood] is the concentration of the dissolved oxygen in the blood plasma, which, according to Henry's law, is in proportion to the oxygen partial pressure p_{ox} as

$$c = \alpha p_{ox} \tag{12}$$

where α [m^3ox/m^3blood Pa] is the oxygen solubility in the blood.

The source term So accounts for the exchange rate between the hemoglobin bound oxygen and dissolved oxygen, as the hemoglobin releases back into the blood plasma due to the reduced oxygen partial pressure. The oxygen passing through a hollow fiber diffuses through the

membrane wall of the hollow fiber to the blood plasma and red blood cells. The diffused oxygen dissolves in the blood plasma flowing over the shell side of the hollow fibers. The binding process takes place between hemoglobin and oxygen molecules. This process is so fast that the degree of oxygen bound to hemoglobin can be expressed as the oxygen saturation S which solely depends on the partial pressure of the oxygen p_{ox} as described by the Hill equation, namely,

$$S(p_{ox}) = \frac{\left(p_{ox}/p_{ref}\right)^n}{1+\left(p_{ox}/p_{ref}\right)^n} \tag{13a}$$

or

$$S(c) = \frac{\left(c/c_{ref}\right)^n}{1+\left(c/c_{ref}\right)^n} \tag{13b}$$

where

$$c_{ref} = \alpha p_{ref} \tag{14}$$

n is the empirical exponent while p_{ref} is the reference partial pressure such that $S(p_{ref}) = 0.5$. Both of these empirical values can be determined for a particular blood condition by correlating the experimental data with the foregoing Hill equation.

Assuming the red blood cells are distributed evenly in blood space and move at the same speed as the blood plasma, the source term So may be given by the Lagrangian derivative of the hemoglobin bound oxygen concentration:

$$So = -\left(\frac{\partial [c]_H S(c)}{\partial t} + \frac{\partial u_j [c]_H S(c)}{\partial x_j}\right) \tag{15}$$

where $[c]_H$ [m^3Hb/m^3blood Pa] is the hemoglobin concentration. Equation (15) may readily be substituted into Eq. (11).

The governing Eqs. (9)–(11) may be decomposed according to Eq. (3). Then, these microscopic equations are integrated over the local control volume, exploiting the foregoing spatial average relationships. The set of the macroscopic governing equations thus obtained for the blood (shell) flow may be given as follows:

$$\frac{\partial \varepsilon_b \langle u_j \rangle^b}{\partial x_j} = 0 \tag{16}$$

$$\begin{aligned}\rho_b \frac{\partial \langle u_i \rangle^b}{\partial t} + \rho_b \frac{\partial \langle u_j \rangle^b \langle u_i \rangle^b}{\partial x_j} &= -\frac{\partial \langle p \rangle^b}{\partial x_i} + \frac{\partial}{\partial x_j}\left(\mu \frac{\partial \langle u_i \rangle^b}{\partial x_j} - \rho \langle \tilde{u}_i \tilde{u}_j \rangle^b\right) \\ &\quad + \frac{1}{V_b}\int_{A_{b_{\text{int}}}} \left(\mu \frac{\partial u_i}{\partial x_j} - p\delta_{ij}\right) n_{bj} dA\end{aligned} \tag{17}$$

$$\begin{aligned}&\frac{\partial \varepsilon_b \left(\langle c \rangle^b + [c]_H \langle S \rangle^b\right)}{\partial t} + \frac{\partial \varepsilon_b \langle u_j \rangle^b \left(\langle c \rangle^b + [c]_H \langle S \rangle^b\right)}{\partial x_j} \\ &= \frac{\partial}{\partial x_j}\left(\varepsilon_b D_b \frac{\partial \langle c \rangle^b}{\partial x_j} + \frac{D_b}{V}\int_{A_{b_{\text{int}}}} c n_{b_j} dA - \varepsilon_b \langle (\tilde{c} + [c]_H \tilde{S}) \tilde{u}_j \rangle^b\right) \\ &\quad + \frac{1}{V}\int_{A_{b_{\text{int}}}} D_b \frac{\partial c}{\partial x_j} n_{bj} dA\end{aligned} \tag{18}$$

where the superscript b is assigned to indicate the blood phase intrinsic average quantities as defined by Eq. (2). Note that n_{bi} is the unit vector pointing outward from the blood side to membrane side and that some surface integral terms have disappeared due to the no-slip conditions. Obviously, the parenthetical terms including the dispersive flux term $-\varepsilon_b \langle (\tilde{c} + [c]_H \tilde{S}) \tilde{u}_j \rangle^b$ on the right hand-side of Eq. (18) denote the diffusive oxygen transfer, while the last term describes the interfacial oxygen transfer between the blood plasma and membrane.

4 Closure for the set of volume averaged equations

The foregoing volume averaged macroscopic Eqs. (16)–(18) may be modeled as follows:

$$\frac{\partial \varepsilon_b \langle u_j \rangle^b}{\partial x_j} = 0 \tag{19}$$

$$\begin{aligned}\rho_b \left(\frac{\partial \langle u_i \rangle^b}{\partial t} + \frac{\partial \langle u_j \rangle^b \langle u_i \rangle^b}{\partial x_j}\right) &= -\frac{\partial \langle p \rangle^b}{\partial x_i} + \mu_b \frac{\partial^2 \langle u_i \rangle^b}{\partial x_j^2} \\ &\quad - \frac{\mu_b}{K_{b_{ij}}} \varepsilon_b \langle u_j \rangle^b\end{aligned} \tag{20}$$

$$\begin{aligned}&\varepsilon_b \left(1 + [c]_H S'\right)\left(\frac{\partial \langle c \rangle^b}{\partial t} + \frac{\partial \langle u_j \rangle^b \langle c \rangle^b}{\partial x_j}\right) \\ &= \frac{\partial}{\partial x_j}\left(\varepsilon_b D_b \frac{\partial \langle c \rangle^b}{\partial x_j} + \varepsilon_b D_{b\,dis_{jk}} \left(1 + [c]_H S'\right) \frac{\partial \langle c \rangle^b}{\partial x_k}\right) \\ &\quad - a_b h_{tb}\left(\langle c \rangle^b - \langle c \rangle^m\right)\end{aligned} \tag{21}$$

where

$$S' \equiv \left.\frac{dS}{dc}\right|_{c=\langle c \rangle^b} = \frac{n\left(\langle c \rangle^b / c_{ref}\right)^{n-1}}{c_{ref}\left(1 + \left(\langle c \rangle^b / c_{ref}\right)^n\right)^2} \tag{22}$$

The concentration on the blood-membrane interface is assumed to be locally uniform such that its surface integral related to the tortuosity:

$$\frac{D_b}{V}\int\limits_{A_{b_{\text{int}}}} c n_{b_j} dA$$

vanishes.

As for the macroscopic momentum equation, the Forchheimer extended Darcy expression may be introduced for the flow resistance in place of the Darcy expression:

$$\frac{1}{V_b}\int\limits_{A_{b_{\text{int}}}} \left(\mu_b \frac{\partial u_i}{\partial x_j} - p\delta_{ij}\right) n_{bj} dA - \frac{\partial}{\partial x_j}\left(\rho_b \langle \tilde{u}_i \tilde{u}_j \rangle^b\right) = -\frac{\mu_b}{K_{b_{ij}}} \varepsilon_b \langle u_j \rangle^b - \rho_b b_{ij} \sqrt{\langle u_k \rangle^b \langle u_k \rangle^b} \langle u_j \rangle^b \tag{23}$$

where the permeability tensor is given by

$$\frac{1}{K_{b_{ij}}} = \begin{bmatrix} \frac{1}{K_{b\,xx}} & 0 & 0 \\ 0 & \frac{1}{K_{b\,yy}} & 0 \\ 0 & 0 & \frac{1}{K_{b\,zz}} \end{bmatrix} \tag{24}$$

The axial permeability component may be evaluated using the hydraulic diameter concept as

$$K_{b_{xx}} = \frac{\varepsilon_b}{32}\left(4\left(\frac{\pi d_b^2}{4(1-\varepsilon_b)}\right)\Big/ \pi d_b\right)^2 = \frac{\varepsilon_b}{32}\left(\frac{d_b}{1-\varepsilon_b}\right)^2 \tag{25}$$

while the transverse components may be estimated according to Kuwahara et al. [15] as

$$K_{b_{yy}} = K_{b_{zz}} = \frac{\varepsilon_b^3}{120}\left(\frac{d_b}{1-\varepsilon_b}\right)^2 \tag{26}$$

Modeling of the Forchheimer tensor b_{ij} for anisotropic structure, however, is not straightforward. For highly non-Darcian flows, one may resort to the procedure introduced by Nakayama et al. [16]. The dispersion oxygen flux, $\varepsilon_b\langle(\tilde{c} + [c]_H \tilde{S})\tilde{u}_j\rangle^b$, may be modeled according to the gradient diffusion hypothesis introduced by Nakayama et al. [17] as

$$-\varepsilon_b\langle(\tilde{c} + [c]_H \tilde{S})\tilde{u}_j\rangle^b = \varepsilon_b D_{dis_{jk}} \frac{\partial}{\partial x_k}\left(\langle c\rangle^b + [c]_H \langle S\rangle^b\right) = \varepsilon_b D_{dis_{jk}}\left(1 + [c]_H S'\right)\frac{\partial \langle c\rangle^b}{\partial x_k} \tag{27}$$

The axial dispersion diffusivity component may be estimated using the hydraulic concept [15, 17] as

$$D_{b\,dis_{xx}} = 2.55\left(\frac{\langle u\rangle^b d_b}{2(1-\varepsilon_b)D_b}\right)^{7/8} Sc_b^{1/8} D_b \tag{28a}$$

for parallel flows

$$D_{b\,dis_{xx}} = 0.05(1-\varepsilon_b)^{1/2}\langle u\rangle^b d_b \quad \text{for cross flows} \tag{28b}$$

The transverse dispersion diffusivity components $D_{d\,dis_{yy}}$ and $D_{d\,dis_{zz}}$ are usually as small as 1/20 of the axial dispersion counterpart [18–20], but, are still much larger than the molecular counterpart D_b.

For the interfacial oxygen transfer, the effective oxygen transfer coefficient on the shell side may be introduced as

$$\frac{1}{V}\int\limits_{A_{b_{\text{int}}}} D_b \frac{\partial c}{\partial x_j} n_{bj} dA = a_b h_{t\,b}\left(\langle c\rangle^b - \langle c\rangle^m\right) \tag{29}$$

where the effective oxygen transfer coefficient $h_{t\,b}$ for the case of negligible tortuosity within the membrane is defined, referring to Fig. 3, as

$$\frac{1}{h_{t\,b}} = \frac{1}{h_b} + \frac{d_b}{2\varepsilon_p D_m}\ln\left(\frac{2d_b}{d_b + d_{ox}}\right) = \frac{1}{h_b} + \frac{d_b}{2\varepsilon_p D_m}\ln\left(\frac{1}{1-\frac{t_m}{d_b}}\right) \tag{30}$$

where D_m is the effective membrane diffusion coefficient and ε_p(0.3–0.5) is the intrinsic porosity of the membrane. According to Hewitt et al. [3], the shell side transfer coefficient may be given as follows:

$$\frac{h_b d_b}{D_b} = 0.524\left(\frac{|\langle \vec{u}\rangle^b| d_b}{\nu_b}\right)^{0.523} Sc_b^{1/3} \tag{31}$$

where $Sc_b = \nu_b / D_b$ is the Schmidt number of the dissolved oxygen in the blood. Note that the shell side transfer coefficient depends locally on the blood velocity field within the chamber, to be determined by solving Eqs. (19) and (20).

Likewise, the set of the macroscopic equations for the oxygen (lumen) flow may be written with sub and superscripts ox. Since the oxygen flow though hollow fibers is unidirectional, the velocity and concentration fields may be approximated by laminar fully developed solutions as

$$\frac{\partial \varepsilon_{ox}\langle u\rangle^{ox}}{\partial x} = 0 \tag{32}$$

$$\rho_{ox}\frac{\partial \langle u_i\rangle^{ox}}{\partial t} = -\frac{\partial \langle p\rangle^{ox}}{\partial x} - 32\frac{\mu_{ox}}{d_{ox}^2}\langle u\rangle^{ox} \tag{33}$$

$$\frac{\partial \varepsilon_{ox}\langle c\rangle^{ox}}{\partial t} + \varepsilon_{ox}\langle u\rangle^{ox}\frac{\partial \langle c\rangle^{ox}}{\partial x} = -a_d h_{t\,ox}\left(\langle c\rangle^{ox} - \langle c\rangle^m\right) \tag{34}$$

Referring to Fig. 3, the interfacial convective transfer between the membrane and the oxygen flow is modeled as

$$\frac{1}{V}\int\limits_{A_{ox\,\text{int}}} D_{ox}\frac{\partial c}{\partial x_j} n_{oxj} dA = a_{ox} h_{t\,ox}\left(\langle c\rangle^{ox} - \langle c\rangle^m\right) \tag{35}$$

where

$$\frac{1}{h_{t_{ox}}} = \frac{1}{h_{ox}} + \frac{d_{ox}}{2\varepsilon_p D_m}\ln\left(\frac{d_b + d_{ox}}{2d_{ox}}\right) = \frac{1}{h_{ox}} + \frac{d_b}{2\varepsilon_p D_m}\left(1 - 2\frac{t_m}{d_b}\right)\ln\left(\frac{1-\frac{t_m}{d_b}}{1-2\frac{t_m}{d_b}}\right) \tag{36}$$

Since the oxygen flow within hollow fibers is likely to be laminar, the lumen side transfer coefficient h_{ox} may be estimated as

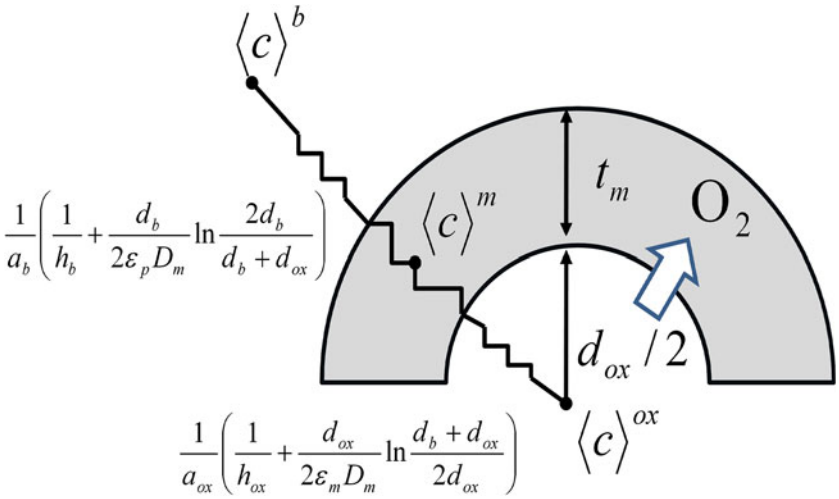

Fig. 3 Diffusion through a membrane

$$\frac{h_{ox}d_{ox}}{D_{ox}} \cong 4 \tag{37}$$

Note that h_{ox} is quite large since d_{ox} is very small.

Since the hollow membranes are made from hydrophobic polymers, the membrane wall pores are constantly filled with oxygen gas supplied by the oxygen flow in the hollow fibers. Naturally, the oxygen gas within the membrane stays still. Thus, as for the membrane phase, one only needs to consider the species concentration equation:

$$\frac{\partial \varepsilon_m \langle c \rangle^m}{\partial t} = a_b h_{t_b}\left(\langle c \rangle^b - \langle c \rangle^m\right) + a_{ox}h_{t\,ox}(\langle c \rangle^{ox} - \langle c \rangle^m) \tag{38}$$

This completes the closure procedure. The present volume average model consists of the continuity, momentum and concentration equations for the blood and oxygen compartments (19), (20), (21), (32), (33), (34), and the concentration equation for the membrane (38). These partial differential equations can be solved numerically for given initial and boundary conditions using any standard numerical procedure such as those based on primitive variables (e.g. Nakayama [9]).

5 Approximate solutions for the unidirectional flow oxygenator with sufficient oxygen supply

Further simplification is possible as one notes the difference in the mass transfer resistances among the blood plasma, membrane and oxygen phases. The total resistance associated with this oxygen transport between the oxygen and blood plasma streams may be split into two parts, as illustrated in Fig. 3. Since the hydrophobic hollow membranes wall pores constantly trap oxygen molecules supplied by the oxygen stream in the hollow fiber, the mass transfer resistance of the lumen side (i.e. the oxygen stream and membrane) is much smaller than that of the shell side (i.e. the blood plasma stream and membrane), namely, $1/a_b h_{t\,b} \gg 1/a_{ox}h_{t\,ox}$. Thus, Eq. (38) for the case of steady state gives

$$\langle c \rangle^m = \frac{a_b h_{t\,b}\langle c \rangle^b + a_{ox}h_{t\,ox}\langle c \rangle^{ox}}{a_b h_{t\,b} + a_{ox}h_{t\,ox}} \cong \langle c \rangle^{ox} \tag{39}$$

One may also note the following scale magnitudes among the three time scales, namely, the convective time scale from the membrane to the blood plasma $1/a_b h_b$, the diffusive time scale within the membrane t_m^2/D_m and the convective time scale from the oxygen stream to the membrane $1/a_{ox}h_{ox}$:

$$1/a_b h_b \gg t_m^2/D_m \gg 1/a_{ox}h_{ox} \tag{40}$$

Therefore, in most membrane blood oxygenators with sufficient supply of the oxygen of $\langle c \rangle^{ox}_{\text{sup}}$, one may assume

$$\langle c \rangle^m \cong \langle c \rangle^{ox} \cong \langle c \rangle^{ox}_{\text{sup}} \tag{41}$$

For the steady unidirectional blood flow in the oxygenator, Eqs. (19) and (20) readily give the Darcian blood velocity and intrinsic blood pressure as

$$u_b \equiv \varepsilon_b \langle u \rangle^b = \text{const.} \tag{42}$$

and

$$-\frac{d\langle p \rangle^b}{dx} = \frac{\mu_b}{\frac{\varepsilon_b}{32}\left(\frac{d_b}{1-\varepsilon_b}\right)^2}u_b = \text{const.} \quad : \text{parallel flows} \tag{43a}$$

$$-\frac{d\langle p \rangle^b}{dx} = \frac{\mu_b}{\frac{\varepsilon_b^3}{120}\left(\frac{d_b}{1-\varepsilon_b}\right)^2}u_b = \text{const.} \quad : \text{cross flows} \tag{43b}$$

Hence, the oxygen transport equation simplifies as follows:

$$u_b\left(1+[c]_H S'\right)\frac{d\langle c\rangle^b}{dx}=\frac{d}{dx}\varepsilon_b\left(D_b+D_{b\,dis}\left(1+[c]_H S'\right)\right)\frac{d\langle c\rangle^b}{dx}-h_{bv}\left(\langle c\rangle^b-\langle c\rangle^{ox}_{\sup}\right) \tag{44}$$

where $h_{bv}=a_b h_b$ is the shell side volumetric transfer coefficient. Upon noting $D_{b\,dis}\gg D_d$, Eq. (44) may be written as

$$u_b\frac{d\langle c\rangle^b}{dx}=\frac{1}{\left(1+[c]_H S'\right)}\frac{d}{dx}\varepsilon_b D_{b\,dis}\left(1+[c]_H S'\right)\frac{d\langle c\rangle^b}{dx}-\frac{h_{bv}}{\left(1+[c]_H S'\right)}\left(\langle c\rangle^b-\langle c\rangle^{ox}_{\sup}\right) \tag{45}$$

Many researchers including Vaslef et al. [21] and Zhang et al. [14] introduced "effective diffusivity" $D_b/(1+[c]_H S')$ to account the oxygen uptake by hemoglobin. However, this definition is not relevant, since the foregoing equation suggests $\varepsilon_b D_{b\,dis}\left(1+[c]_H S'\right)/\left(1+[c]_H S'\right)=\varepsilon_b D_{b\,dis}$ when the local variation of $\left(1+[c]_H S'\right)$ is neglected. The effects of the mechanical dispersion on the diffusivity are neglected in most previous investigations. But, it is the dispersion that controls the diffusive mechanism in the oxygen transport in membrane oxygenators.

The transport equation derived for the membrane oxygenation devices may readily be translated for the oxygen transport equation in biological systems. For human respiratory system with low blood velocity in capillary vessels, on the other hand, Taylor dispersion [22] prevails such that $D_{dis}/D_b\sim(u_b d_b/D_b)^2$. Since the Peclet number $u_b d_b/D_b$ in capillary vessels can be as small as unity, the molecular diffusion is as important as the mechanical dispersion. Thus, the full ordinary differential Eq. (44) should be used to describe the oxygen transport in biological systems with the effective diffusivity being $\varepsilon_b(D_{b\,dis}+D_b/\left(1+[c]_H S'\right))$.

Returning back to oxygenators, Eq. (45) may be rewritten in a dimensionless form as

$$\frac{d^2c^*}{dx^{*2}}=-\frac{[c]^*_H S^{*\prime\prime}}{1+[c]^*_H S^{*\prime}}\left(\frac{dc^*}{dx^*}\right)^2+Na\left(\frac{dc^*}{dx^*}+\frac{c^*-c^*_{\sup}}{1+[c]^*_H S^{*\prime}}\right) \tag{46}$$

where

$$c^*=\frac{\langle c\rangle^b}{c_{ref}}=\frac{\langle p_{ox}\rangle^b}{p_{ref}} \tag{47}$$

such that

$$c^*_{\sup}=\frac{\langle c\rangle^{ox}_{\sup}}{c_{ref}}=\frac{p_{ox_{\sup}}}{p_{ref}}\quad\text{and}\quad [c]^*_H=\frac{[c]_H}{c_{ref}}=\frac{[c]_H}{\alpha p_{ref}} \tag{48a, b}$$

$$x^*=\frac{h_{bv}x}{u_b} \tag{49}$$

$$S^{*\prime}=\frac{dS^*}{dx^*}=\frac{nc^{*n-1}}{\left(1+c^{*n}\right)^2} \tag{50}$$

$$S^{*\prime\prime}=\frac{d^2S^*}{dx^{*2}}=\frac{nc^{*n-2}(n-1-(n+1)c^{*n})}{\left(1+c^{*n}\right)^3} \tag{51}$$

and

$$Na\equiv\frac{u_b^2}{\varepsilon_b D_{b\,dis}h_{bv}} \tag{52}$$

is the square of the mass transfer version of the dimensionless number introduced by Nakayama [23], namely, $\frac{u}{\alpha_{eff}}\sqrt{\frac{k_{eff}}{h_v}}$ where $\alpha_{eff}(\sim\varepsilon_b D_{b\,dis})$, $h_v(\sim h_{bv}k_{eff}/\varepsilon_b D_{b\,dis})$ and k_{eff} are the effective thermal diffusivity, volumetric heat transfer coefficient and effective thermal conductivity. This dimensionless number measures the distance which the oxygen gas travels to dissolve in the blood stream u_b/h_{bv}, referring as to the dispersion mixing length $\varepsilon_b D_{b\,dis}/u_b$. For usual oxygenators, Na number is sufficiently large as can be evaluated using Eqs. (28a, 28b) and (31) as

$$Na\equiv\frac{u_b^2}{\varepsilon_b D_{b\,dis}h_{bv}}=0.34\frac{\varepsilon_b}{(1-\varepsilon_b)^{1/8}}\left(\frac{u_b d_b}{\varepsilon_b \nu_b}\right)^{0.6}Sc_b^{2/3}\quad\text{for parallel flows} \tag{53a}$$

$$Na\equiv\frac{u_b^2}{\varepsilon_b D_{b\,dis}h_{bv}}=9.52\frac{\varepsilon_b}{(1-\varepsilon_b)^{2/3}}\left(\frac{u_b d_b}{\varepsilon_b \nu_b}\right)^{0.477}Sc_b^{2/3}\quad\text{for cross flows} \tag{53b}$$

For human respiratory system with low blood velocity in capillary vessels, on the other hand, one may estimate as

$$Na\equiv\frac{u_b^2}{\varepsilon_b D_{b\,dis}h_{bv}}\sim\frac{u_b^2}{\varepsilon_b\left(u_b^2 d_b^2/D_b\right)h_{bv}}\sim\frac{D_b}{h_v d_b}\sim\frac{1}{Sh_b} \tag{54}$$

Naturally, Na number, which is inversely proportional to the Sherwood number, can be so small that the diffusion terms must be retained for the case of human respiratory system.The second order ordinary differential Eq. (46) may easily be solved using a standard integration scheme such as Runge–Kutta–Gill (e.g. [9]) with the following boundary conditions:

$$x^*=0: c^*=\frac{\langle c\rangle^b_{in}}{c_{ref}}=\frac{p_{ox\,in}}{p_{ref}}\quad\text{and}\quad\frac{d^2c^*}{dx^{*2}}=0 \tag{55a, b}$$

Note that x^* is the dimensionless coordinate with its reference length u_b/h_{bv} being approximately the distance which the oxygen molecules travel till they dissolve in the

blood plasma. Thus, when designing a compact oxygenator, one should ensure that this dimensionless length $L^* = h_{bv}L/u_b$ stays within the order of unity under all possible operating conditions. This point will be discussed later in connection with oxygenator efficiency. Note that Eq. (55b) together with Eq. (46) yields a quadratic equation with respect to the first derivative dc^*/dx^*, which can be solved to provide the boundary value for dc^*/dx^* at $x^* = 0$.

6 Results and discussion

Zhang et al. [14] carried out an experimental investigation using a custom-made mini-oxygenator, which was placed in a parallel flow chamber. A flat fiber membrane bundle of 12.7 mm (height) × 45.72 mm (width) × 50.4 mm (length) was placed in cross flow arrangement, in which the fibers are perpendicular to the blood flow. The following input data needed for the analysis were collected from their paper:

$p_{ref} = 29\,\text{mmHg}$ $(c_{ref} = 8.7 \times 10^{-4}\text{m}^3\text{ox}/\text{m}^3\,\text{blood})$, $\alpha = 3.0 \times 10^{-5}\,\text{m}^3\text{ox}/\text{m}^3\text{blood mmHg}$, $n = 2.84$, $[c]_H = 0.166\,\text{m}^3\text{Hb}/\text{m}^3\text{blood Pa}$, $p_{ox\,in} = 40\,\text{mmHg}$, $p_{ox\,\sup} = 760\,\text{mmHg}$, $\varepsilon_b = 0.6$, $d_b = 300 \times 10^{-6}\,\text{m}$, $v_b = 2.76 \times 10^{-6}\,\text{m}^2/\text{s}$, $D_b = 1.8 \times 10^{-9}\,\text{m}^2/\text{s}$, $A = 5.81 \times 10^{-4}\,\text{m}^2$, $L = 0.0504\,\text{m}$, $a_b = 5,810/\text{m}$.

The corresponding dimensionless parameters are as follows:

$$[c]^*_H = 191,\ c^*_{\sup} = 26.2,\ c^*(0) = 1.38,\ Sc_b = 1,530$$

The integration should be carried out from $x^* = 0$ to $x^* = L^*$. For example, L^* in the case of the blood volume flow rate $Q_b = Au_b = 1\,\text{l/min}$ $(\text{i.e.}\,u_b = 0.0287\,\text{m/s})$ is given by

$$L^* = \frac{h_{bv}L}{u_b} = 0.524\frac{a_bL}{\varepsilon_b\left(\frac{u_bd_b}{\varepsilon_bv_b}\right)^{0.477}Sc_b^{2/3}} = 0.877 \tag{56}$$

Furthermore, Eq. (53b) reveals that $Na = 3{,}070$ is so large that the diffusion terms in Eq. (47) may well be neglected as

$$\frac{dc^*}{dx^*} = \frac{c^*_{\sup} - c^*}{1 + [c]^*_H S^{*\prime}} = \frac{c^*_{\sup} - c^*}{1 + [c]^*_H \frac{nc^{*n-1}}{(1+c^{*n})^2}} : Na \gg 1 \tag{57}$$

Once $c^*(L^*)$ is known, one can easily obtain the total oxygen transfer rate $Q_{ox}[\text{m}^3/\text{s}]$ from

$$Q_{ox} = Q_bc_{ref}\left\{c^*(L^*) - c^*(0) + [c]^*_H(S(c^*(L^*)) - S(c^*(0)))\right\} \tag{58}$$

In Fig. 4, the total oxygen transfer rates predicted from the foregoing first order ordinary differential Eq. (57) without the diffusion terms are compared against those obtained from the complete second order ordinary differential Eq. (57) for $Na = 0.01$, 0.1, 1 and 5. The figure shows that the results for the case of $L^* > 5$ are almost identical to those obtained without the diffusion terms ($Na = \infty$). Thus, in most cases, the first order ordinary equation suffices for practical estimations.

Zhang et al. [14] conducted a series of measurements using bovine bloods. They collected pressure drop and oxygen transfer rate data using the aforementioned custom-made mini-oxygenator and the Medtronic Affinity NT oxygenator (Medtronic Inc., Minneapolis, MN, USA), in which the hollow fiber bundle is arranged in an annulus with its inner and outer diameters being 0.0318 and 0.0762 m, respectively. In the Medtronic Affinity NT oxygenator, the blood fluid particles enter through the core of the oxygenator chamber and then make turn to pass radially crossing over the bundle of the hollow fibers. The specifications of the Medtronic Affinity NT oxygenator are given as follows:

$$\varepsilon_b = 0.45,\quad A \cong 0.080\pi\frac{0.0762 + 0.0318}{2} = 0.0136\,\text{m}^2,$$
$$L = \frac{0.0762 - 0.0318}{2} = 0.0222\,\text{m},\quad a_b = 9,260/\text{m}.$$

The other parameters and properties are the same as the case of the custom-made mini-oxygenator. The average blood velocity in the Medtronic Affinity NT oxygenator is estimated by dividing the volume blood flow rate by the average area A available for the transverse flow, according to Hewitt et al. [3].

The pressure drops are presented in Fig. 5, in which the experimentally measured data are compared against the present correlation given by Eq. (43b). The experimentally measured pressure drops for both oxygenators, in a low

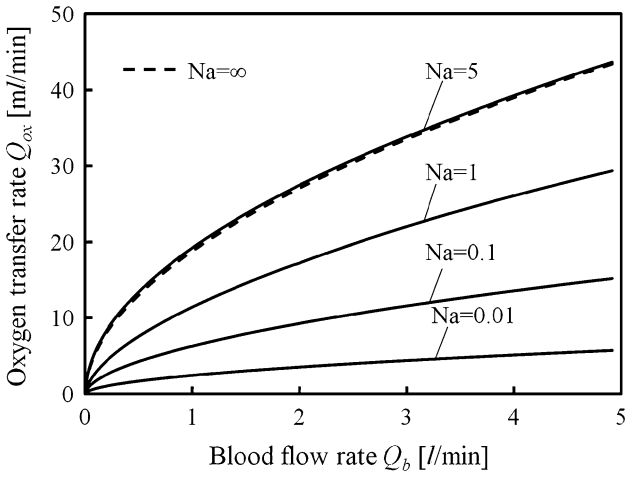

Fig. 4 Effects of Na on dissolved oxygen concentration, $Na = 0.01$, 0.1, 1 and 5, Custom-made mini-oxygenator, Technical data are taken from Zhang et al. [14]

flow rate range, are in reasonable agreement with the present theoretical correlation. However, in a high flow rate range, the inertia effects on the pressure drops become significant, resulting in higher pressure drops. Such inertia effects may be implemented by introducing the Forchheimer term (i.e. the velocity square term) as given by Eq. (23).

In the Medtronic Affinity NT oxygenator, the fluid particles path length L is estimated as half the difference between the outer and inner diameters of the fiber bundle. Thus, the dimensionless length L^* based on Eq. (56) for the case of the blood volume flow rate $Q_b = 1\,\mathrm{l/min}$ (i.e. $u_b = 0.00123\,\mathrm{m/s}$) may be estimated by $L^* = 3.22$.

The oxygenator efficiency may be defined as follows:

$$\eta_{th}(L^*) \equiv \frac{Q_{ox}}{Q_{ox\,th}} = \frac{Ah_{b\,v}\int_0^L \left(c_{\mathrm{sup}} - \langle c\rangle^b\right)dx}{Ah_{b_{b\,v}}\int_0^\infty \left(c_{\mathrm{sup}} - \langle c\rangle^b\right)dx} = \frac{\int_0^{L^*}\left(c^*_{\mathrm{sup}} - c^*\right)dx^*}{\int_0^\infty \left(c^*_{\mathrm{sup}} - c^*\right)dx^*} \tag{59}$$

which indicates the ratio of the oxygen transfer rate with the effective flow path length L to the maximum oxygen transfer rate with an infinite flow path length, for fixed blood flow rate Q_b. Figure 6 shows the oxygenator efficiency as function of the dimensionless length L^*. The efficiency increases with L^* and approaches 100 % asymptotically. The efficiency of 90 % reaches at the dimensionless length 3.5. A further increase in L^* beyond this value would not be justified since the concentration difference $\left(c_{\mathrm{sup}} - \langle c\rangle^b\right)$ is too small to gain substantial oxygen transfer. Moreover, a device with L^* much smaller than 3.5 may not either be justified since the concentration difference is still large such that additional oxygen transfer would be possible by providing an additional flow path. In reality, the blood flow rate must be controlled with the other parameters fixed. Therefore, one should design an oxygenator such that L^* stays around 3 to maintain high efficiency under possible operating conditions. The efficiency curve may roughly be approximated as

$$\eta_{th}(L^*) = \begin{cases} L^*/3.2 & : L^* \le 3.2 \\ 1 & : L^* \ge 3.2 \end{cases} \tag{60}$$

Hence,

$$Q_{ox} = \eta_{th} Q_{ox\,th} \cong \begin{cases} 0.0692 Q_b (L^*/3.2) & : L^* \le 3.2 \\ 0.0692 Q_b & : L^* \ge 3.2 \end{cases} \tag{61a, b}$$

where

$$Q_{ox\,th} = Ah_{b\,v}\int_0^\infty \left(c_{\mathrm{sup}} - \langle c\rangle^b\right)dx = \left(c_{ref}\int_0^\infty \left(c^*_{\mathrm{sup}} - c^*\right)dx^*\right) Q_b = 0.0692 Q_b \tag{62}$$

It is interesting to note that the proportional relationship as given by Eq. (61b) holds for all efficient oxygenators with sufficiently large membrane surface areas, operated with bovine bloods under $p_{ox\,in} = 40\,\mathrm{mmHg}$, $p_{ox\,\mathrm{sup}} = 760$ mmHg, irrespective of other technical specifications of the devices in use.

Figure 7(a) shows the total oxygen transfer rates calculated from Eq. (58), using the present analytical results, together with the experimentally measured transfer rates at different blood flow rates for both oxygenators. The dimensionless length L^*, which decreases with increasing the blood flow rate, was evaluated using Eq. (56). The present analysis correctly shows a plateau at a higher blood flow rate range as experimentally observed for the custom-

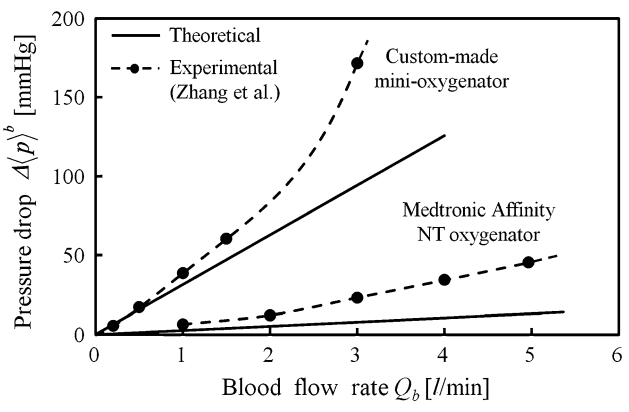

Fig. 5 Comparison of pressure drops, Custom-made mini-oxygenator and Medtronic Affinity NT oxygenator, Technical data are taken from Zhang et al. [14]

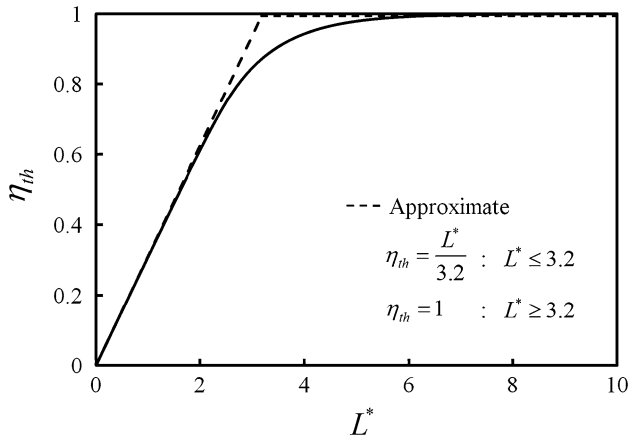

Fig. 6 Oxygenator efficiency, Bovine blood with $p_{ox\,in} = 40\,\mathrm{mmHg}$ and $p_{ox\,\mathrm{sup}} = 760\,\mathrm{mmHg}$

made mini-oxygenator. It, however, underestimates the total oxygen transfer rate. In the same figure, the analytical results based on McAdams' mass transfer correlation [24] are also presented for comparison:

$$\frac{h_b d_b}{D_b} = \left(0.35 + 0.56\left(\frac{u_b d_b}{\varepsilon_b \nu_b}\right)^{0.52}\right) Sc_b^{0.3} : \text{McAdams} \quad (63)$$

The results indicate that the mass transfer coefficient has significant influence on the total oxygen transfer rate, and thus, must be evaluated carefully depending on a particular flow field. The experimentally measured oxygen transfer rate in the Medtronic Affinity NT oxygenator in the high flow rate range is much higher than the one based on the analysis, since the flow in this range is no longer radial but quite three-dimensional, as manifested by the nonlinear increase in the pressure drops in Fig. 5. Such three-dimensional mixing enhances the mass transfer rate such that the dimensionless length proportional to the volumetric heat transfer coefficient may well be $L^* \geq 3.2$. Thus, Eq. (61b) valid for $L^* \geq 3.2$ is plotted in the same figure, which shows a good agreement with the experimental data for the case of the Medtronic Affinity NT oxygenator.

The simple proportional relationship valid for devices with sufficiently large membrane surface areas, as given by Eq. (61b), is examined against the experimental data by provided by Matsuda et al. [25] who used the membrane oxygenator, HPO-25H, Senko Medical Instrument, with bovine bloods. Unfortunately, sufficient technical data on this particular membrane oxygenator and experimental conditions are not available from their paper. Assuming that all operations with their oxygenator device were made with sufficiently large dimensionless length $L^* \geq 3.2$, the linear relationship given by Eq. (61b) is presented along with their experimental data in Fig. 7b. A reasonable agreement between the prediction and experiment can be seen from the figure.

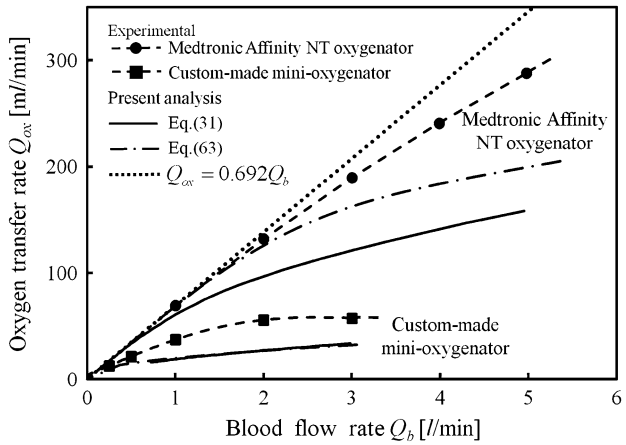

(a) Experimental data from Zhang et al. [14]

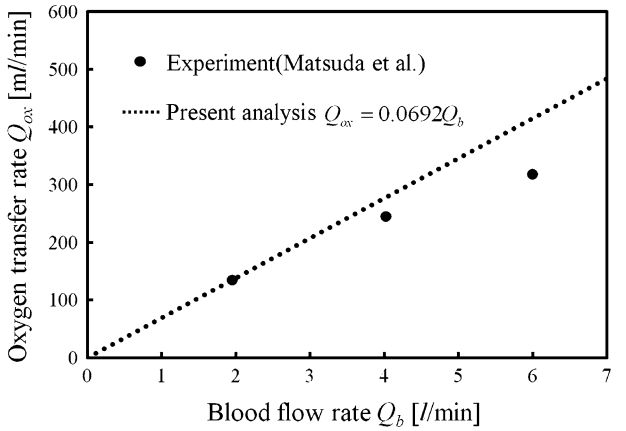

(b) Experimental data from Matsuda et al. [25]

Fig. 7 Comparison of total oxygen transfer rates **a** experimental data from Zhang et al. [14], **b** experimental data from Matsuda et al. [25]

7 Conclusions

A volume averaging theory has been adopted to derive a set of the macroscopic governing equations for characterizing the oxygen transport processes within membrane blood oxygenation devices. The derived equations indicate that the dispersion coefficient corresponds to an effective diffusion coefficient for the oxygen transport in oxygenators. A scale analysis was also made on the resulting oxygen transport equation, defining a dimensionless number which measures the distance the oxygen gas travels to dissolve in the blood as compared with the blood dispersion length. The analysis reveals that the effects of diffusive terms on the development of the oxygen concentration are negligibly small. The analytical results obtained based on a unidirectional flow assumption are compared with experimentally measured pressure drops and total oxygen transfer rates for both custom-made mini-oxygenator and Medtronic Affinity NT oxygenator. A simple linear relationship between the blood flow rate and total oxygen transfer rate is found for oxygenators with sufficiently large membrane surface areas. The agreement observed between the analysis and experiment reveals the validity of the present approach based on the porous media theory. A series of numerical calculations using the full three-dimensional set of the governing equations are being conducted in the authors' group, so as to consider possible optimization of compact oxygenators. The results will be published in near future.

Acknowledgments The authors gratefully acknowledge invaluable technical supports provided by Mr. R. Imai, Department head of Clinical Engineering, Shizuoka Institute of Medical Care Science.

References

1. Guzman AM, Escobar RA, Amon CH (2005) Flow mixing enhancement from balloon pulsations in an intravenous oxygenator. ASME J Biomech Eng 127:400–415
2. Guzman AM, Escobar RA, Amon CH (2005) Methodology for predicting oxygen transport on an intravenous membrane computational and analytical models. ASME J Biomech Eng 127:1127–1140
3. Hewitt TJ, Hattler BG, Federspiel WJ (1998) A mathematical model of gas exchange in an intravenous membrane oxygenator. Ann Biomed Eng 26:166–178
4. Hewitt TJ, Hattler BG, Federspiel WJ (2000) Experimental evaluation of a model for oxygen exchange in a pulsating intravascular artificial lung. Ann Biomed Eng 28:160–167
5. Federspiel WJ, Golob JF, Frankowski BJ, Merrill TL, Litwak K, Hattler BG (1999) Development and testing of an intravascular artificial ling. In: Proceedings of the annual international conference of the IEEE engineering in Medicine and Biology, vol 1, p 345
6. Federspiel WJ, Hewitt TJ, Hattler BG (2000) Experimental evaluation of a model for oxygen exchange in a pulsating intravascular artificial lung. Ann Biomed Eng 28:160–167
7. Cheng P (1978) Heat transfer in geothermal systems, Advances in Heat Transfer, vol 14. Academic Press, New York, pp 1–105
8. Quintard M, Whitaker S (1993) One and two equation models for transient diffusion processes in two-phase systems. Adv Heat Transf 23:369–465
9. Nakayama A (1995) PC-aided numerical heat transfer and convective flow. CRC Press, Boca Raton
10. Vafai K, Tien CL (1981) Boundary and inertia effects on flow and heat transfer in porous media. Int J Heat Mass Transf 24:195–203
11. Nakayama A, Kuwahara F (2008) A general bioheat transfer model based on the theory of porous media. Int J Heat Mass Transf 51:3190–3199
12. Sano Y, Nakayama A (2012) A porous media approach for analyzing a countercurrent dialyzer system. ASME J Heat Transf 134:072602. doi:10.1115/1.4006104
13. Catapano G, Papenfuss HD, Wodetzki A, Baurmeister U (2001) Mass and momentum transport in extra-luminal flow (ELF) membrane devices for blood oxygenation. J Membr Sci 175: 97–110
14. Zhang J, Nolan TDC, Zhang T, Griffith P, Wu ZJ (2007) Characterization of membrane blood oxygenation devices using computational fluid dynamics. J Memb Sci 288:268–279
15. Kuwahara F, Nakayama A, Koyama H (1996) A numerical study of thermal dispersion in porous media. J Heat Transf 118: 756–761
16. Nakayama A, Kuwahara F, Hayashi T (2004) Numerical modeling for three-dimensional heat and fluid flow through a bank of cylinders in yaw. J Fluid Mech 498:139–159
17. Nakayama A, Kuwahara F, Kodama Y (2006) An equation for thermal dispersion flux transport and its mathematical modelling for heat and fluid flow in a porous medium. J Fluid Mech 563:81–96
18. Yang C, Kuwahara F, Liu W, Nakayama A (2011) Thermal nonequilibrium forced convective flow in an annulus filled with a porous medium. Open Transp Phenom J 3:31–39
19. Yang C, Liu W, Nakayama A (2009) Forced convective heat transfer enhancement in a tube with its core partially filled with a porous medium. Open Transp Phenom J 1:1–6
20. Yang C, Nakayama A (2010) A synthesis of tortuosity and dispersion in effective thermal conductivity. Int J Heat Mass Transf 53:3222–3230
21. Vaslef SN, Mockros LF, Anderson RW, Leonard RJ (1994) Use of a mathematical model to predict oxygen transfer rates in hollow fiber membrane oxygenators. ASAIO J 40:990–996
22. Taylor GI (1953) Dispersion of solute matter in solvent flowing slowly through a tube. Proc R Soc Lond 15(1953):1787–1806
23. Nakayama A, Kuwahara F, Sugiyama M, Xu GL (2001) A two-energy equation model for conduction and convection in porous media. Int J Heat Mass Transf 44:4375–4379
24. McAdams WH (1954) Heat transmission, 3rd edn. McGraw Hill, New York, pp 266–268
25. Matsuda N, Nakamura M, Sakai K, Kuwana K, Tahara K (1999) Theoretical and experimental evaluation for blood pressure drop and oxygen transfer rate in outside blood flow membrane oxygenator. J Chem Eng Japan 32:752–759